ADVANCED MATERIALS INTERFACES
www.advmatinterfaces.de

Check for updates

Interaction of Water with Atomic Layer Deposited Titanium Dioxide on p-Si Photocathode: Modeling of Photoelectrochemical Interfaces in Ultrahigh Vacuum with Cryo-Photoelectron Spectroscopy

Thorsten Cottre, Mathias Fingerle, Melanie Kranz, Thomas Mayer, Bernhard Kaiser,* and Wolfram Jaegermann*

This study combines cryo-photoelectron spectroscopy and electrochemical analysis techniques to investigate the p-Si/SiO_2/TiO_2/H_2O system in the context of water-splitting. Atomic layer deposition is used for the preparation of a TiO_2 thin film coating for a p-Si/SiO_2 photocathode. First, an interface experiment is performed to study the contact properties of the interface between p-Si/SiO_2 and TiO_2. For the p-Si/TiO_2 heterojunction, a downward band bending of 0.3 eV is found for the p-Si toward the interface. Second, a water adsorption experiment is conducted, which allows the investigation of the surface chemistry of the TiO_2 coating in contact to water. A direct correlation between the amount of surface hydroxide species, formed due to water dissociation, and Ti^{3+} defect state density is found. Furthermore, a surface water species can be identified in addition to the commonly found bulk molecular water. Together with the results from a Mott–Schottky analysis, a complete energy level alignment can be constructed.

1. Introduction

The production of sustainable hydrogen via photoelectrochemical water-splitting is a promising energy storage technology. Besides the development of efficient photoabsorbers and the design of advanced electrocatalysts, a fundamental understanding of the semiconductor/electrolyte interface on an atomic scale is needed.[1]

Titanium dioxide is a wide-bandgap semiconductor with outstanding properties. The high dielectric constant,[2,3] the high refractive index[4] and an optical transparency in the visible range[5] as well as photocatalytic properties[6] are valuable for technological applications in the field of electronics, optics and catalysis. Moreover, titanium dioxide fulfills the criteria as a passivation layer, due to its chemical stability in aqueous electrolyte solutions and the sufficient electronic conductivity, induced by intrinsic n-doping.[7] Besides the protection against corrosion, recent studies confirm that a surface passivation in general can also suppress charge recombination and improve the reaction kinetics due to a better charge separation.[8,9]

Thin films of TiO_2 can be prepared by various conventional deposition techniques like physical vapor deposition (PVD)[10–12] and chemical vapor deposition (CVD),[13,14] as well as by atomic layer deposition (ALD), which has different advantages due to the self-limited process as follows:

Atomic layer deposition has developed to be the key technology for the deposition of various oxides in the recent years.[15] On the basis of the unique process control by alternating exposure of the precursors, ALD offers the possibility to produce high conformal thin films with an exact layer thickness. Furthermore, the process not only enables the deposition of flat substrates, but also of complex materials with a high aspect ratio.[16]

In general, the stability of photoelectrodes is strongly affected by degradation processes on the device surface. Especially the possibility of photocorrosion initialized by excited charge carriers is an important aspect in this context and leads to unwanted side reactions to the hydrogen evolution reaction (HER).[8,17] Our last study highlighted the correlation between the electronic structure and the photoelectrochemical characteristic of integrated Si-based devices for solar-driven water-splitting.[18] ALD-TiO_2 layers served as a surface passivation and Pt particles were added as an active electrocatalyst. During longer process times a degradation process was observed, which lowers the overall efficiency of the prepared devices. A post-mortem analysis with electron microscopy gave insight into the degradation mechanism which shows a higher tendency to occur at chemical inhomogeneities.[19] In addition to impurities at the surface of the material, the photoactivity of TiO_2 is

T. Cottre, Dr. M. Fingerle, M. Kranz, Dr. T. Mayer, Dr. B. Kaiser, Prof. W. Jaegermann
Surface Science Group
Materials Science Department
Technical University of Darmstadt
Otto-Berndt-Str. 3, 64287 Darmstadt, Germany
E-mail: mayerth@surface.tu-darmstadt.de; kaiser@surface.tu-darmstadt.de

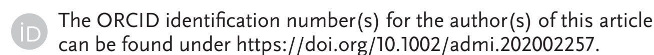
The ORCID identification number(s) for the author(s) of this article can be found under https://doi.org/10.1002/admi.202002257.

© 2021 The Authors. Advanced Materials Interfaces published by Wiley-VCH GmbH. This is an open access article under the terms of the Creative Commons Attribution License, which permits use, distribution and reproduction in any medium, provided the original work is properly cited.

DOI: 10.1002/admi.202002257

 © 2021 The Authors. Advanced Materials Interfaces published by Wiley-VCH GmbH

21967350, 2021, 11, Downloaded from https://onlinelibrary.wiley.com/doi/10.1002/admi.202002257 by Technische Universitat Darmstadt, Wiley Online Library on [12/02/2024]. See the Terms and Conditions (https://onlinelibrary.wiley.com/terms-and-conditions) on Wiley Online Library for rules of use; OA articles are governed by the applicable Creative Commons License

a plausible explanation for the formation of Ti^{3+} defects at the surface, which can initialize the observed degradation mechanism.[20–22] However, the exact origin of the defect formation at the semiconductor/electrolyte interface is still not fully understood. Our approach uses cryo-photoelectron spectroscopy for the modeling of photoelectrochemistry in ultrahigh vacuum to get an insight in the defect formation.

In the present study, we investigate the p-Si/SiO_2/TiO_2/H_2O model system with regard to water-splitting and application for the hydrogen evolution reaction side on a fundamental level. Using a surface science approach, we derive the energy level alignment throughout the complete system. The first part of this study focuses on the ALD-coating of the p-Si/SiO_2 photocathode with TiO_2, which is investigated via conventional X-ray photoelectron spectroscopy (XPS). For the second part, the investigation of the p-Si/SiO_2/TiO_2 system with regard to water-splitting, we conduct a water adsorption experiment in the so-called frozen electrolyte approach. For various metal oxides, the frozen electrolyte approach has already been successfully applied in the past.[23–25]

In general, surface science studies on interfaces in contact with water are suffering from the so called "pressure-gap": Water vapor or even fluid water is not accessible with standard XPS, which is limited to UHV conditions. But especially in the field of photoelectrochemistry, where the basic mechanisms of water-splitting are induced by the respective contact between metal oxide interface and water, these types of studies are most relevant. Currently, two options are available: 1) Ambient-pressure photoelectron spectroscopy[26] and 2) cryo-photoelectron spectroscopy, where the pressure gap is overcome by studying a frozen water film and therefore the UHV during analysis can be maintained.

On an LN-cooled manipulator, we perform cryo-photoelectron spectroscopy, employing X-rays (Cryo-XPS) as well as UV light (Cryo-UPS) as excitation source, and combine the results with electrochemical Mott–Schottky analysis for the description of the band alignment situation in the p-Si/SiO_2/TiO_2 system during contact to an electrolyte. With this strategy the surface chemistry during electrolyte contact can be investigated and the influence on the electronic structure can be studied on the atomic scale.

2. Results and Discussion

2.1. Formation of the p-Si/SiO_2/TiO_2 Interface

During ALD-growth of the TiO_2 layer, each cycle deposits a certain amount of TiO_2 on the p-Si/SiO_2 substrate. To conduct the interface experiment, consecutive measurements were done after 25, 50, 75, 100 and 300 cycles. The development of the core-level XP spectra and the valence band spectra upon stepwise ALD-TiO_2 deposition is depicted in **Figure 1a**.

In the O1s spectra a clear transition from SiO_2 with an initial binding energy of 533.0 eV to TiO_2 at a final position of 530.6 eV can be observed. Furthermore, the stepwise deposition of ALD-TiO_2 leads to an increase of the Ti2p and a decrease of the Si2p intensity. Noticeably, an incorporation of chlorine in the formed TiO_2 film can be detected. This can be explained by Ti-Cl surface species formed in the first half-cycle of the ALD-process, which did not react with water via a ligand exchange in the second half-cycle. Additionally, the dissociative re-adsorption of HCl on the oxygen bridges during both half-cycles of the ALD process can lead to chlorine impurities.[27] Although a N_2 purging was used to remove the HCl gas efficiently, the chlorine content in the films is about 2% at. conc.

The development of the valence band spectra during the interface experiment shows a superposition of the p-Si/SiO_2 and the TiO_2 signal. For TiO_2 the valence band is mainly formed by Ti3d-O2p π-bonding states around 5 eV and by O2p-Ti3d σ-bonding states in the range of 8 eV.[28]

The initial growth rate of ALD-TiO_2 on the native oxide of silicon is 0.08 nm/cycle (Figure 1b). In the literature similar values can be found for the precursor system $TiCl_4$/H_2O.[29–31] At the beginning of the deposition a substrate dependent growth inhibition was observed. This can be explained by a difference in the reaction behavior. While on SiO_2 the number of hydroxyl groups on the surface defines saturation, the limiting factor on TiO_2 seems to be the steric hindrance of the chlorine ligands.[27,32,33] Especially the dissociative re-adsorption of HCl can create an additional reaction path for the adsorption of $TiCl_4$ on TiO_2.[27] In contrast to this, the re-adsorption of HCl on SiO_2 does not take place at a growth temperature of 160 °C.[32] Also, the possibility of dissociative and associative adsorption of $TiCl_4$ exists on TiO_2 but not on SiO_2.[27,32,33]

In Figure 1c the changes in binding energy are illustrated for the relevant core-level peaks. While the oxide component of silicon shows a continuous shift to lower binding energies of –0.9 eV in the O1s spectrum and of –0.7 eV in the Si2p spectrum, the elemental silicon peak stabilizes after an initial shift of –0.3 eV. After applying 100 ALD cycles the Ti2p signal shows a small shift of –0.2 eV to lower binding energies at first, but in the last step of the interface experiment the Ti2p signal shifts back and reaches a final value of 459.3 eV for the $Ti2p_{3/2}$ peak maximum. In previous studies we observed a similar behavior and assume that the reversal shift is correlated to the formation of bulk like TiO_2 with oxygen vacancies (Ti_2O_3), which are responsible for an intrinsic n-doping in the material.[34,35] Therefore, the final peak shift is a Fermi-level shift due to n-doping. Furthermore, we assume that the incorporated chlorine impurities additionally enhance the n-doping of the film. Considering the shifts of the elemental component in the Si2p peak and the position of the valence band of the pristine sample as well as the doping concentration in the bulk, a value of 0.3 eV can be calculated for the downward band bending in the p-Si at the interface (see also Figure 7). The energy level alignment at the p-Si/SiO_2/TiO_2 interface will be discussed in more detail in the following, including the evolution upon contact to water.

A more detailed view of the deposited TiO_2 film is given in **Figure 2**. To quantify the amount of the oxygen vacancies a component-fit was performed for the silicon sample deposited with 300 ALD cycles. The main component in the O1s spectrum belongs to TiO_2 and is located at a binding energy of 530.6 eV (Figure 2a). In addition, another component can be identified in the O1s spectrum at 531.6 eV which can be assigned to weakly adsorbed oxygen species, subsurface low-coordinated oxygen ions, surface hydroxyl groups and/or carbonate species.[36] The Ti2p peak (Figure 2b) shows the typical spin-orbit splitting including the $Ti2p_{3/2}$ component at 459.3 eV and the $Ti2p_{1/2}$ component at 465.0 eV for Ti^{4+}. The asymmetry of the peaks reveals the presence of Ti^{3+} located at 458.1 and 463.8 eV.

© 2021 The Authors. Advanced Materials Interfaces published by Wiley-VCH GmbH

21967350, 2021, 11, Downloaded from https://onlinelibrary.wiley.com/doi/10.1002/admi.202002257 by Technische Universitat Darmstadt, Wiley Online Library on [12/02/2024]. See the Terms and Conditions (https://onlinelibrary.wiley.com/terms-and-conditions) on Wiley Online Library for rules of use; OA articles are governed by the applicable Creative Commons License

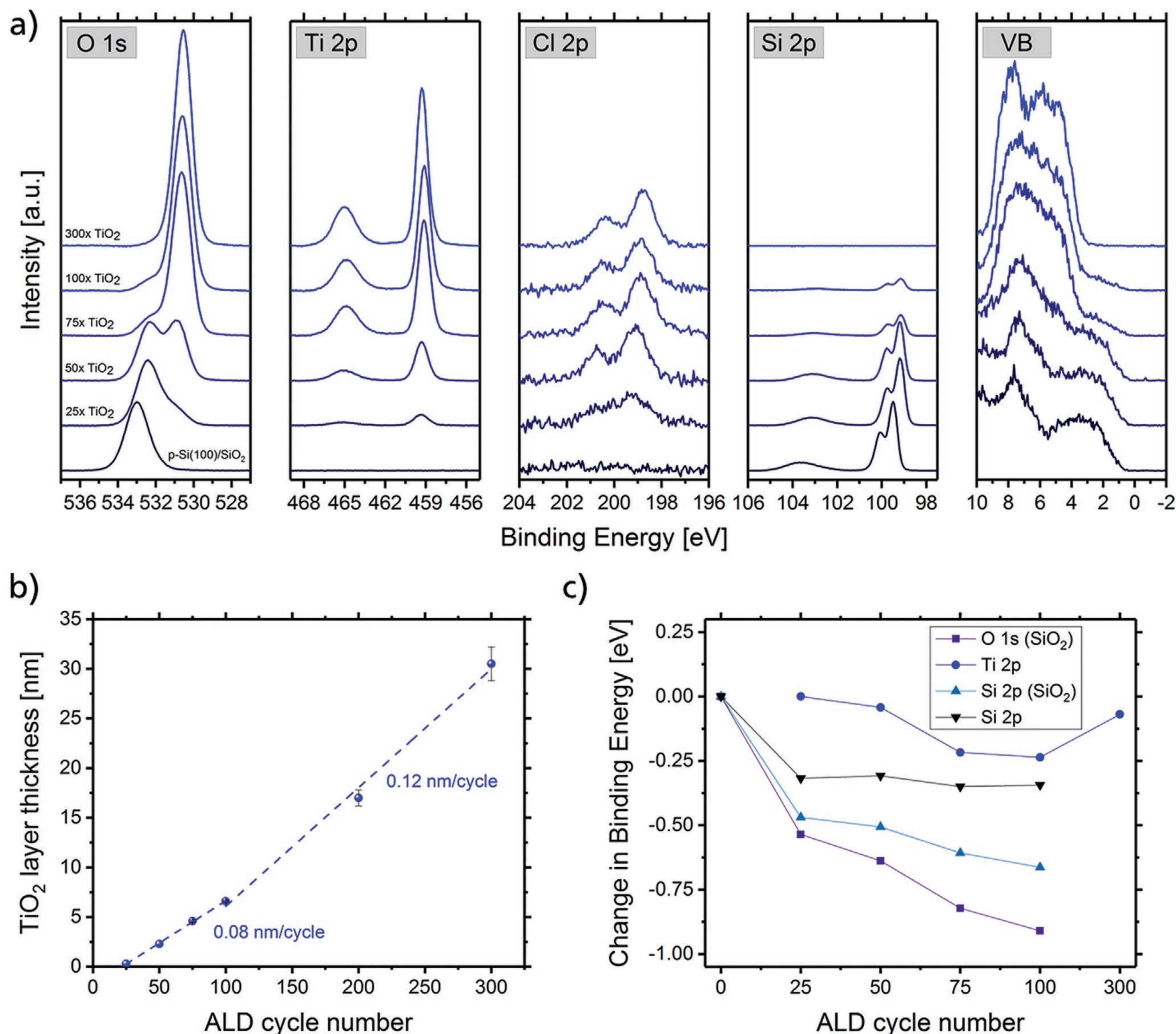

Figure 1. Interface experiment of ALD-TiO_2 on p-Si/SiO_2: a) relevant core-level XP spectra (O1s, Ti2p, Cl2p, and Si2p) and valence band spectra (VB); b) growth rate of ALD-TiO_2 on the native oxide of silicon; c) Change in the O1s, Ti2p, and Si2p core line upon ALD-TiO_2 deposition.

Considering all detected elements, the film after 300 ALD cycles consists of approximately 93% at. conc. TiO_2 as the main component, 5% at. conc. Ti_2O_3 and 2% at. conc. chlorine.

2.2. Mott–Schottky Analysis

For the determination of the flat-band potential V_{fb} and the donor concentration N_D of ALD-TiO_2 a Mott–Schottky analysis was performed using the Mott–Schottky relationship (Equation 1)

$$\frac{1}{C^2} = \frac{2}{\varepsilon\varepsilon_0 e N_D}\left(V - V_{fb} - \frac{k_B T}{e}\right) \quad (1)$$

where C denotes the interfacial capacitance density, ε denotes the dielectric constant of the semiconductor (75 for TiO_2[37]), ε_0 denotes the vacuum permittivity, e denotes the elementary charge, k_B denotes the Boltzmann's constant, and T denotes the temperature (298.15 K). The energy difference between the conduction band E_{CB} and the Fermi-level E_F is calculated using the following relationship (Equation 2)[38]

$$E_{CB} - E_F = \frac{k_B T}{e}\ln\left(\frac{N_C}{N_D}\right) \quad (2)$$

where N_C represents the effective density of states in the conduction band. N_C can be obtained from the relationship given in (Equation 3)[38]

$$N_C = 2\left(\frac{2\pi m_e^* k_B T}{h^2}\right)^{\frac{3}{2}} \quad (3)$$

 © 2021 The Authors. Advanced Materials Interfaces published by Wiley-VCH GmbH

21967350, 2021, 11, Downloaded from https://onlinelibrary.wiley.com/doi/10.1002/admi.202002257 by Technische Universitat Darmstadt, Wiley Online Library on [12/02/2024]. See the Terms and Conditions (https://onlinelibrary.wiley.com/terms-and-conditions) on Wiley Online Library for rules of use; OA articles are governed by the applicable Creative Commons License

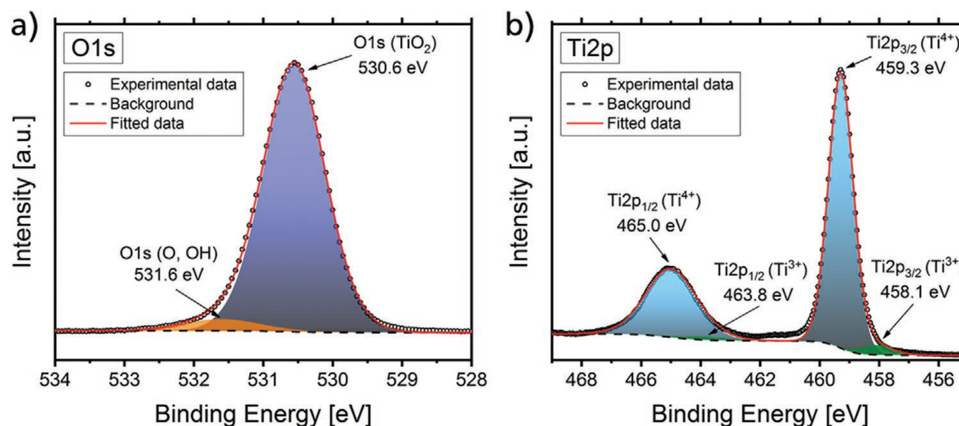

Figure 2. Component-fit of ALD-TiO_2 (30 nm) on p-Si/SiO_2: a) O1s peak (TiO_2: 530.6 eV; O, OH: 531.6 eV), b) Ti2p peak ($Ti2p_{3/2}$ (Ti^{4+}): 459.3 eV; $Ti2p_{1/2}$ (Ti^{4+}): 465.0 eV; $Ti2p_{3/2}$ (Ti^{3+}): 458.1 eV; $Ti2p_{1/2}$ (Ti^{3+}): 463.8 eV).

h is the Plank's constant and m_e^* the effective mass of the electron. Using the assumption that the m_e^* of the amorphous TiO_2 coating is the same as that for TiO_2 in the anatase modification (10 m_e[39]), N_C can be calculated to 7.86×10^{20} cm^{-3}.

To construct the Mott–Schottky plots (**Figure 3a**) for ALD-TiO_2 from the impedance data measured in 0.1 м KOH and 0.1 м H_2SO_4 an equivalent circuit is needed, which describes the system sufficiently. Here a simple equivalent circuit was chosen with the components described in Figure 3b. Under consideration that the width of the space-charge layer is much larger than the width of the Helmholtz layer, C can be extracted directly from the fitted model and treated as the interfacial capacitance density for the space-charge region in TiO_2. The positive slopes indicate a n-doping in the TiO_2, which is in good agreement with the XPS analysis described above.

The flat band potential of ALD-TiO_2 has been determined to 0.14 V versus RHE in 0.1 м KOH and to 0.10 V versus RHE in 0.1 м H_2SO_4 from the respective intersection with the x-axis. The slope of 1.47×10^{11} F^{-2} cm^4 V^{-1} obtained in 0.1 м KOH and of 1.16×10^{11} F^{-2} cm^4 V^{-1} obtained in 0.1 м H_2SO_4 imply that the Fermi-level position is located ≈0.1 eV below the conduction band. The corresponding donor densities for the measurements in 0.1 м KOH and 0.1 м H_2SO_4 are $N_D = 1.28 \times 10^{19}$ cm^{-3} and $N_D = 1.62 \times 10^{19}$ cm^{-3}, respectively. Furthermore, OCP measurements, carried out before the impedance analysis, reveal the position of the Fermi-level in the electrochemical equilibrium at 0.8 V versus RHE in 0.1 м KOH and at 0.4 V versus RHE in 0.1 м H_2SO_4. In summary, the Mott–Schottky analysis indicates a suitable band alignment for the charge transfer needed for the HER.

2.3. Surface Chemistry at the Frozen Electrolyte Interface

For the water adsorption on the p-Si/SiO_2 photocathode coated with TiO_2, a thickness of about 6 nm (100 ALD cycles) was chosen for the metal oxide layer, to be able to still probe the Si2p core level and derive a complete energy level alignment by means of XPS during water adsorption. After cooling the sample down to LN_2-temperature, the asis Cryo-XPS and -UPS measurements of the pristine sample were conducted. Afterward, water was stepwise adsorbed onto the surface, to measure at total nominal doses of 0.1, 0.2, 0.4, 1.6, and 10 L. Afterward, the sample was brought back to room temperature to measure the spectra after desorption.

Of all core levels, the O1s peak holds the most valuable information regarding water adsorption on the p-Si/SiO_2/TiO_2

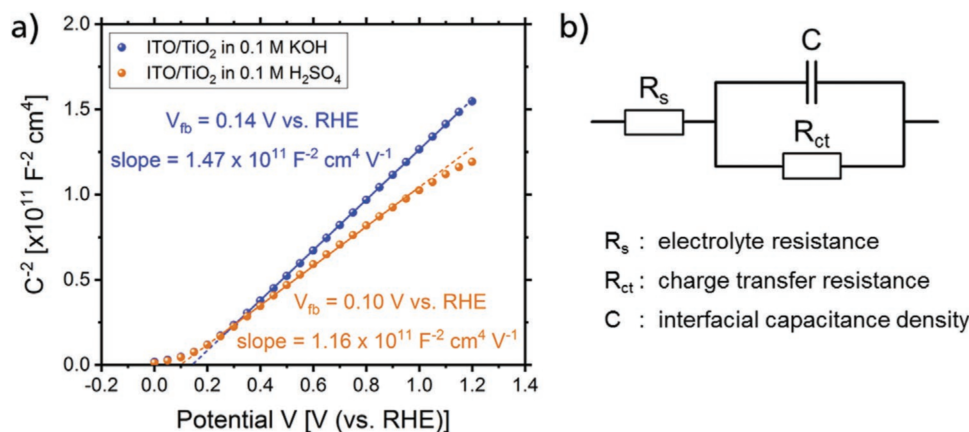

Figure 3. Mott–Schottky analysis: a) Mott–Schottky plot of ALD-TiO_2 on ITO measured in 0.1 м KOH and 0.1 м H_2SO_4; b) equivalent circuit for impedance modeling.

© 2021 The Authors. Advanced Materials Interfaces published by Wiley-VCH GmbH

21967350, 2021, 11, Downloaded from https://onlinelibrary.wiley.com/doi/10.1002/admi.202002257 by Technische Universitat Darmstadt, Wiley Online Library on [12/02/2024]. See the Terms and Conditions (https://onlinelibrary.wiley.com/terms-and-conditions) on Wiley Online Library for rules of use; OA articles are governed by the applicable Creative Commons License

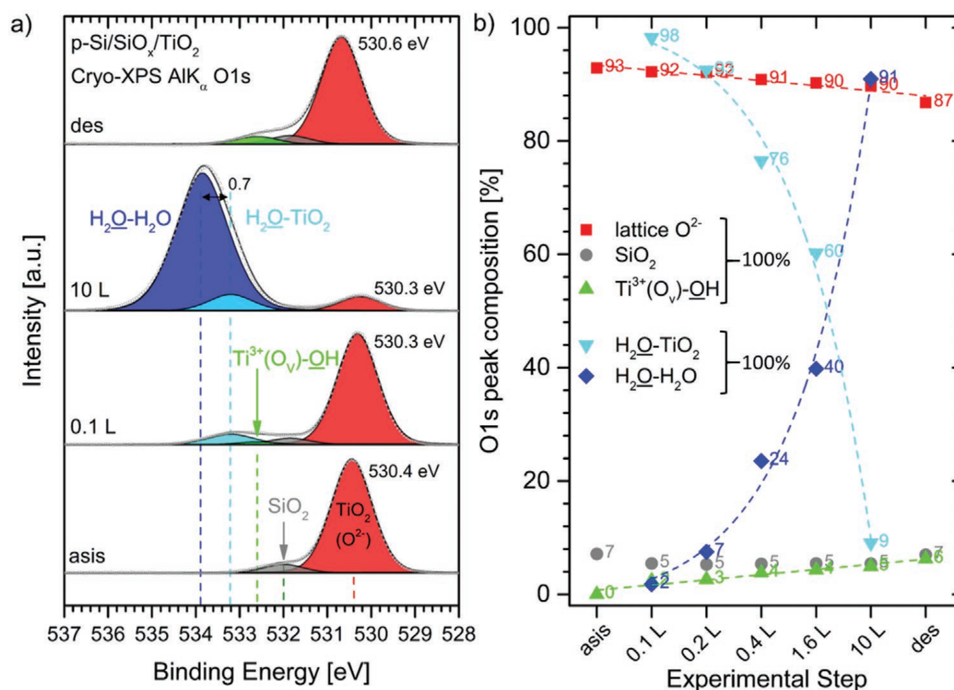

Figure 4. a) Cryo-XPS AlK$_\alpha$ O1s spectra of the subsequential water adsorption on p-Si/SiO$_2$/TiO$_2$, followed by water desorption. b) Percentual O1s peak composition during the water adsorption experiment. The substrate components are monitored in relation to each other, but seperately from the two molecular water species in relation to each other.

photocathode, since the TiO_2 substrate as well as the adsorbing water have a prominent signal in this binding energy region. Moreover, all reaction products (hydroxide species) involve oxygen. Therefore, the O1s core level allows for the detailed observation and quantitative comparison of the surface reactivity upon water adsorption and desorption. **Figure 4a** shows the Cryo-XPS spectra of the pristine TiO_2 as well as for the first (0.1 L) and last (10 L) adsorption step, followed by desorption. The lattice oxygen (O^{2-}) peak of the pristine TiO_2 thin film has a binding energy of 530.4 eV, which has already been reported for an ALD deposited TiO_2 on p-Si with a comparable film thickness.[40] As can be deduced from the interface experiment, the presence of SiO_2 can still be detected in the O1s spectrum at binding energies of 532.0 eV. Recently, in the context of photocatalysis, the role of oxygen vacancies O_v correlated to Ti^{3+} and electronic gap states has been highlighted: Oxygen defective TiO_{2-x} shows an improved solar absorption,[41] wettability[42] and photcalatytic activity.[43,44] After the first adsorption step of 0.1 L water, we assign the small peak at 532.3 eV to basic Ti-OH groups,[44,45] which involve the formation of oxygen vacancies (O_v) at the surface. In Figure 4 we refer to these hydroxyl species as $Ti^{3+}(O_v)$-OH. This is in accordance to an increased intensity of Ti^{3+} in the Ti2p core level (see **Figure 5**) and an increased density of Ti3d gap states in the valence band region (see **Figure 6c**). The formation of this hydroxide species will be discussed in more detail in the following. Lately, we studied the adsorption of water on nickel oxide, where besides molecular water in the common bulk phase, a molecular surface species was found at lower binding energies compared to the bulk phase.[24] In the present experiment on TiO_2, we can again identify such a surface species: After a dose of 0.1 L water, we detect

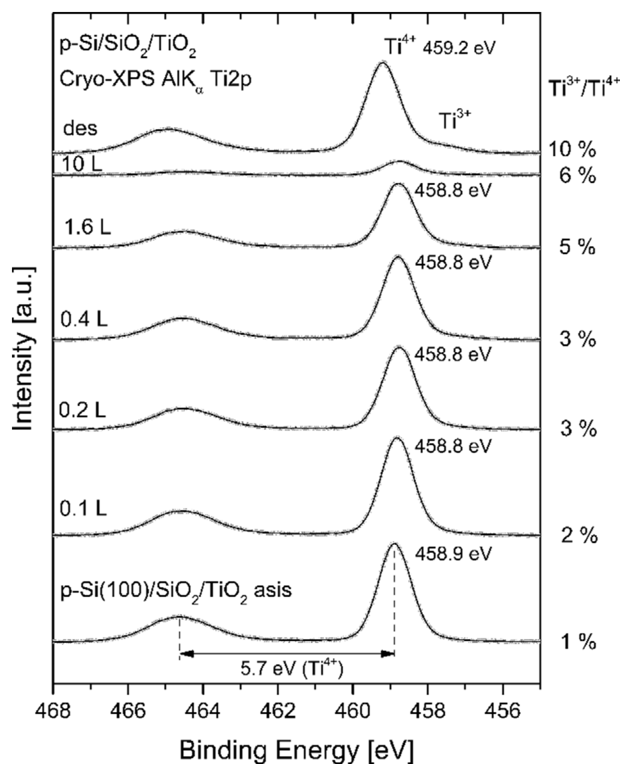

Figure 5. Cryo-XPS AlK$_\alpha$ Ti2p spectra of the subsequential water adsorption on p-Si/SiO$_2$/TiO$_2$, followed by water desorption. Indicated are the binding energies of the $Ti^{4+}2p_{3/2}$ main emission line and the ratio between Ti^{3+} and Ti^{4+} as percentage, calculated by peak fitting (not shown).

 © 2021 The Authors. Advanced Materials Interfaces published by Wiley-VCH GmbH

21967350, 2021, 11, Downloaded from https://onlinelibrary.wiley.com/doi/10.1002/admi.202002257 by Technische Universitat Darmstadt, Wiley Online Library on [12/02/2024]. See the Terms and Conditions (https://onlinelibrary.wiley.com/terms-and-conditions) on Wiley Online Library for rules of use; OA articles are governed by the applicable Creative Commons License

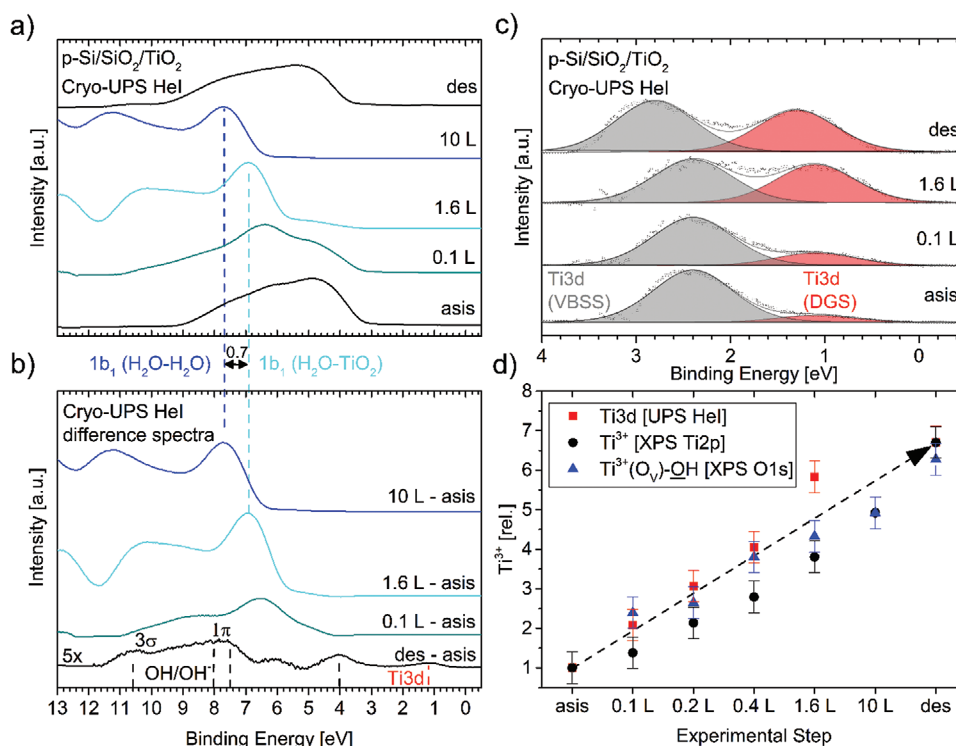

Figure 6. a) Cryo-UPS HeI spectra and b) respective difference spectra as well as c) detailed HeI spectra of the evolution of the Ti^{3+}3d gap state and d) relative increase of the Ti^{3+}3d gap state compared to the increase of Ti^{3+} in the Ti2p core level and the amount of hydroxides in the O1s spectra for the stepwise water adsorption on p-Si/SiO_2/TiO_2 and after desorption.

a new component at 533.2 eV, which we assign to a physisorbed H_2O-TiO_2 species, weakly interacting with the metal oxide surface. Since the chemical reactivity of the TiO_2 upon exposure to water is limited, as additional hydroxide species obviously only form to a very small extent, it is plausible to argue, that most of the water adsorbs molecularly. The interaction of the H_2O with the TiO_2 substrate leads to a lower binding energy value compared to the water bulk phase. The water surface species will cover most of the surface up to a monolayer, while water dissociation leading to $Ti^{3+}(O_V)$-OH species is limited to existing or additionally formed oxygen vacancy sites. For higher doses and water multilayers, we detect the common bulk water species H_2O-H_2O at typical binding energies of 533.9 eV.[46] For the highest dose of 10 L water, the bulk species H_2O-H_2O is dominant, although the surface water layer as well as the TiO_2 substrate can still be detected. The surface species is separated in binding energy by only 0.7 eV, which is comparable to the results on NiO.[24] The nature of this binding energy difference might be related to a (partial) negative charge transfer toward the water, or might be caused by a specific orientation of the water molecules (and therefore molecular dipoles) in contact with the surface, leading to a surface dipole. The presence and relative intensity of these two water species is confirmed by UPS measurements (see Figure 6). The substrate peak O^{2-} as well as the surface hydroxide species $Ti^{3+}(O_V)$-OH show a coordinated shift by 0.1 eV toward lower binding energies in the course of water adsorption. Interestingly, after water desorption, a shift of 0.4 eV toward higher binding energies is observed. The two molecular water species do not follow the coordinated shift to lower binding energies and desorb completely.

The percentual evolution of the O1s components throughout the water adsorption experiment is monitored in Figure 4b. For all adsorption steps, the intensity of the three substrate related components, namely lattice O^{2-}, SiO_2 and chemisorbed OH, is given in relation to each other. The evolution reflects a linear increase of the hydroxide species with increasing water dosage, increasing additionally after desorption. Seperated from the substrate components, the two molecular water species are monitored in Figure 4b in relation to each other. The surface water species H_2O-TiO_2 is the dominant species up to about 1.6 L water dosage. Since 1 L nominally resembles one monolayer, it can be assumed, that after 1.6 L water dosage in the experiment, the first monolayer of water is closed. Due to the fact, that there are minor amounts of bulk water H_2O-H_2O present already for very low doses, it is reasonable to argue, that the water is not exhibiting a perfect layer-by-layer growth. However, after a water dosage of 10 L, the bulk water is the dominant species detected, nearly fully superimposing the signal of the surface water.

The formation of oxygen vacancies at the TiO_2 surface involves a change of oxidation state of the Ti^{4+} to Ti^{3+}. The reduction of Ti atoms can be monitored by recording the Ti2p core level. Figure 5 shows the Cryo-XPS spectra for the Ti2p region for the stepwise water adsorption followed by desorption. The ratio between Ti^{3+} and Ti^{4+} calculated by peak fitting (not shown) is given for each spectrum on the right side. The binding energies found for the $Ti2p_{3/2}$ and $Ti2p_{1/2}$ are 458.9 and 464.6 eV, respectively, and match the values reported for 100 ALD cycles on p-Si[40] as well as commonly expected values for TiO_2 in the Ti^{4+} oxidation state.[45,47] The $Ti2p_{3/2}$ peak exhibits a slight shoulder toward lower binding energies, which

© 2021 The Authors. Advanced Materials Interfaces published by Wiley-VCH GmbH

21967350, 2021, 11, Downloaded from https://onlinelibrary.wiley.com/doi/10.1002/admi.202002257 by Technische Universitat Darmstadt, Wiley Online Library on [12/02/2024]. See the Terms and Conditions (https://onlinelibrary.wiley.com/terms-and-conditions) on Wiley Online Library for rules of use; OA articles are governed by the applicable Creative Commons License

is assigned to the presence of small amounts of Ti^{3+}.[47] In the course of the stepwise water adsorption, the relative amount of Ti^{3+} increases continously, starting from 1% up to 6% and increases further to 10% after water desorption. The binding energy shift of the Ti2p core level is coordinated to the O1s core level shift: In contact to water, a small shift of 0.1 eV toward lower binding energies is observed, while after water desorption, a shift of 0.4 eV to higher binding energies is observed. Taking the change of the work function from 5.1 eV for the pristine TiO_2 to 4.8 eV after desorption into account (see Figure 7), this effect can be attributed to a Fermi-level shift upward, since all core levels, the TiO_2 as well as the Si2p peaks, show the same coordinated shift to higher binding energies. This is equivalent to a n-doping of the TiO_2 layer, due to an increased density of oxygen vacancies at the surface.

In literature, the adsorption of water on TiO_2 single crystals has been widely investigated in terms of crystal orientation and surface defects. On defect free TiO_2 (100),[48,49] TiO_2 (110)[50,51] surfaces, water adsorbs predominantly molecularly, while on TiO_2 (001)[52,53] and on structurally defective surfaces the H_2O dissociation is enhanced.[45,47–60] As relevant defects grain boundaries, step edges and oxygen vacancies have to be considered. In particular, the density of oxygen vacancies plays an important role for the reactivity of the surface.[49,55–57,59] The presence of oxygen vacancies leads to gap states, settled between the valence band maximum of the pristine TiO_2, here at around 3.2 eV, and the Fermi-level E_F. For polycristalline TiO_2 these Ti3d gap states have been widely discussed, although their exact nature is still under debate.[61,62] For single crystals, it is even possible to distinguish between deep gap states (DGS) and shallow gap states (SGS).[1,63,64] The latter presumably occurs on step edges of the surface. Lately, a theoretically reported valence band surface state (VBSS)[65] has also been resolved experimentally.[66]

In Figure 6a, the UPS HeI spectra of the pristine TiO_2 thin film as well as after 0.1, 1.6, and 10 L water adsorption as well as after desorption are shown. Additionally, in Figure 6b, the respective difference spectra to the asis spectrum are shown. The valence band spectrum of the pristine TiO_2 thin film is in very good agreement to literature.[67] With a valence band edge at 3.2 eV and the presence of Ti3d deep gap states at 1.1 eV it reflects a n-type TiO_2. We tentatively assign the hole transport inside the bandgap to specific electronic properties of the resulting defect states. Already after 0.1 L water adsorption, the typical fingerprint of molecular water is visible in the respective difference spectra. The $1b_1$ peak maximum has a binding energy of 6.5 eV. With increasing water adsorption up to 1.6 L, the H_2O features become more distinct. The 10 L difference spectrum is shifted 0.7 eV to higher binding energies compared to the 1.6 L spectrum and shows broader features. It can be concluded, that the 10 L difference spectrum shows a mixed phase of two species: The first with a $1b_1$ peak maximum at 6.5 eV is dominant for lower water doses, while the second with a $1b_1$ peak maximum at 7.2 eV is dominant for higher doses. In fact, two different water species on a metal oxide surface are already known in literature,[68] specifically for TiO_2[69] as well as lately for nickel oxide.[24] The features of the first species, detected in the (sub)monolayer range, exhibit a lower binding energy than usually found for molecular water, just as for the O1s core level spectra. The water molecules are directly physisorbed on the TiO_2 surface and the molecular interaction with the metal oxide surface lowers the ionization potential of the water molecules (see Figure 7). The second species, dominant in the multilayer range, has typical binding energies (and ionization potential) of molecular H_2O-H_2O water in the bulk phase. After desorption, we detect only chemisorbed hydroxide species to a minor extent on the surface, which can be deduced from the respective difference spectrum, which has been multiplied with a factor of 5 to visualize the residuals. The chemisorbed species show the typical signature of OH (at 7.5 and 10.6 eV) and OH^- (at 8.1 and 10.6 eV).[70] The feature at around 4 eV might as well be related to hydroxide surface species,[46,68] or result from changes of nonbonding O2p states of the TiO_2 valence band. However, it has to be noted again, that the intensity of the additional hydroxide species is very low, as already deduced from the Cyro-XPS O1s core level. At 1.1 eV, an enhanced intensity of Ti3d gap states after desorption is clearly visible in the difference spectrum. The origin of the Ti3d gap states has been controversely discussed, claiming that the intensity of the gap states is either proportional to the presence of oxygen vacancies[62] or to Ti interstitials.[61] In Figure 6c, the UPS HeI band gap region is shown with a fit of two different gap states: A peak with a maximum at 1.1 eV, which we assign as Ti3d deep gap state (DGS),[64] as well as a peak with a maximum at 2.4 eV, which we assign as a valence band surface state (VBSS).[66] In the asis spectrum, the Ti3d peak is present only to a minor extent. This changes upon water adsorption, as the DGS intensity increases proportional to the water dosage relative to the VBSS intensity. After desorption, the intensity of the DGS is almost seven times higher compared to the asis spectrum. And comparing the relative intensity increase over the experiment to the ratio of Ti^{3+} detected in the Ti2p core level, as plotted in Figure 6d, we can assume, that the Ti3d deep gap states are directly related to Ti^{3+}, since they show the same linear trend. As the nature of the Ti3d gap state is still under debate, it can only be speculated about the detailed chemical and structural interpretation in this case. Qualitatively, the chemical reactions at the surface due to water chemisorption lead to oxygen vacancies and the formation of Ti^{3+} and therefore the gap states seem to be proportional to oxygen vacancies rather than propertional to Ti interstitials.

2.4. Energy Level Alignment Based on the Frozen Electrolyte Approach

The energy level alignment of a comparable interface, p^+-Si covered with ALD-TiO_2, has already been studied by means of XPS/UPS.[71] But in contrast to the present study, the silicon substrates were pretreated with the RCA cleaning procedure. The ALD-TiO_2 deposition leads to a flat-band situation in the p^+-Si and the formation of a $Si_xTi_yO_2$ interlayer. In contrast to this, the downward band bending in the p-Si observed in the present case favors electron transport across the interface. Water adsorption on TiO_2 rutile and nanoparticles has been studied,[26,72] but so far the discussion on band alignment has been limited to the interaction between TiO_2 and water. To our best knowledge, this study is the first to discuss the energy level alignment of the complete $Si/SiO_2/TiO_2/H_2O$ system.

© 2021 The Authors. Advanced Materials Interfaces published by Wiley-VCH GmbH

21967350, 2021, 11, Downloaded from https://onlinelibrary.wiley.com/doi/10.1002/admi.202002257 by Technische Universitat Darmstadt, Wiley Online Library on [12/02/2024]. See the Terms and Conditions (https://onlinelibrary.wiley.com/terms-and-conditions) on Wiley Online Library for rules of use; OA articles are governed by the applicable Creative Commons License

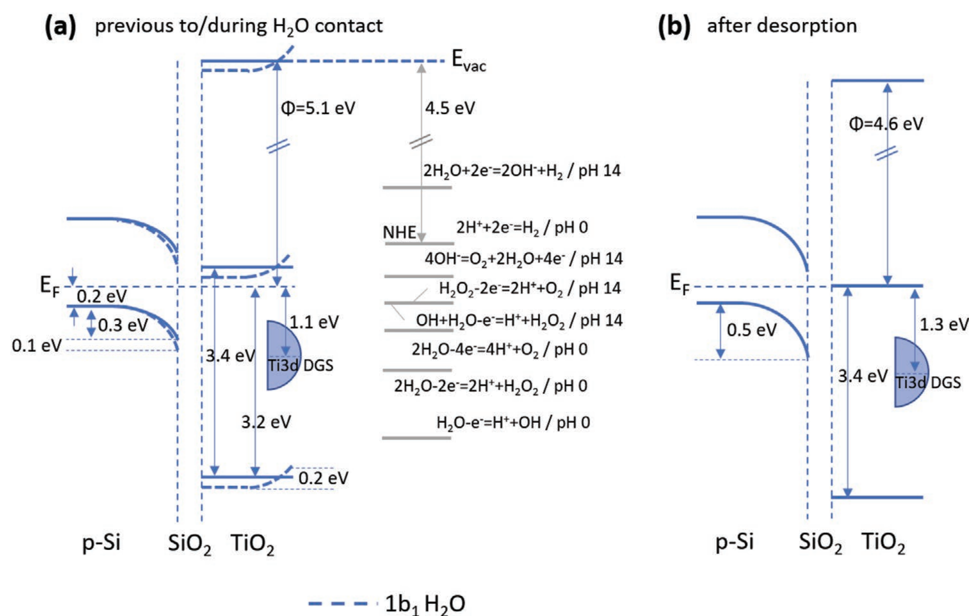

Figure 7. Energy level alignment of the p-Si/SiO_2/TiO_2 photocathode before and during water adsorption in relation to a) the redox potentials of the H_2O catalysis as well as b) after water desorption. The reversible band bending upon water adsorption is indicated in (a) as dashed lines.

Figure 7a schematically draws the band diagram of the p-Si/SiO_2/TiO_2 photocathode previous to and during contact to water. The thickness of the intermediate SiO_2 layer is about 2 nm which enables tunneling processes across the interface. Based on the peak maximum of the Si2$p_{3/2}$ peak at 99.4 eV (see Figure S1, Supporting Information) and a valence band maximum of 5.5 eV derived from the respective UPS HeI spectrum, the band bending at the p-Si/SiO_2 interface can evaluated to be 0.3 eV, considering the bulk position of the valence band maximum according to doping concentration and the measured position. The ALD TiO_2 thin film has a thickness of about 6 nm. The valence band maximum is measured ca. 3.2 eV below the Fermi-level E_F and the work function was calculated from the secondary electron onset (not shown in the spectra) to be Φ_{TiO2} = 5.1 eV. Upon water adsorption, gradual energy level shifts were detected in the range of 100 meV. However, while the Si2p core level shifts 0.1 eV to higher binding energies, the TiO_2 core level shift 0.1 eV to lower binding energies. This means that the water induced band bending at the TiO_2/H_2O interface adds up to about 0.2 eV. The energy level positions and band bending during contact to water is indicated as dashed lines in Figure 7a. Based on the Ti2p spectra in Figure 1 we assume that there is a small band bending upward (≈25 meV) in the TiO_2 toward the interface to SiO_2 present. But since the extent of the measured band bending is below the energetic resolution of the XPS the band bending is not shown in Figure 7.

In our Mott–Schottky analysis which we performed ex situ on a 30 nm thick TiO_2 film in contact with liquid electrolyte solution (0.1 M potassium hydroxide solution and 0.1 M sulfuric acid solution) we have found that the width of the depletion layer toward the water exceeds the layer thickness of the 6 nm thick TiO_2 film in the cryo-experiment. In the course of the water adsorption on the 6 nm TiO_2 thin film we observe an increase of oxygen defects which is correlated to the Ti^{3+} defect density (see Figure 6d). We therefore assume that the resulting band bending is in the dimension of the layer thickness. H. Yang et al. highlighted the importance of thin film thickness with respect to the electrical and optical properties of TiO_2.[73] For the adsorption experiment in this study, the layer thickness of 6 nm was chosen to allow the acquisition of the Si2p core level. However, based on this energy level alignment, a detailed parameter study of thin film thickness would be of interest to investigate the changes in the electronic structure but exceeds the focus of the given study.

After water desorption the band bending of TiO_2 toward the frozen electrolyte layer is fully reversed. The opposing peak shift of the Si/SiO_2 toward the thin metal oxide overlayer has already been observed for nickel oxide on n-Si[24] in contact to water and is possibly a general effect for Si/SiO_2 systems covered with thin MeO_x films. After water desorption, a coordinated shift of 0.4 eV to higher binding energies of all core levels as well as of the valence band is observed. As already discussed, this effect can be attributed to a Fermi-level shift upward, which is equivalent to a n-doping of the TiO_2 layer, due to an increased density of oxygen vacancies at the surface. This effects the p-Si as well, and increases the band bending downward toward the SiO_2 interlayer from 0.3 to 0.5 eV, as shown in Figure 7b. The Fermi-level is then settled directly at the conduction band edge of the TiO_2.

Figure 8 shows the evolution of the work function as well as the ionization potential (IP) of the two detected water species. While the $IP_{H2O-H2O}$ = 11.8 eV of the bulk water species is a well known value, the $IP_{H2O-Ti2O}$ = 11.2 eV of the surface species is lower, due to the molecular interaction of the H_2O with the metal oxide surface. The work function decreases from 5.1 eV for pristine TiO_2 to 4.3 eV for a surface covered with a surface water film. The difference of 0.8 eV in work function matches

 © 2021 The Authors. Advanced Materials Interfaces published by Wiley-VCH GmbH

21967350, 2021, 11, Downloaded from https://onlinelibrary.wiley.com/doi/10.1002/admi.202002257 by Technische Universitat Darmstadt, Wiley Online Library on [12/02/2024]. See the Terms and Conditions (https://onlinelibrary.wiley.com/terms-and-conditions) on Wiley Online Library for rules of use; OA articles are governed by the applicable Creative Commons License

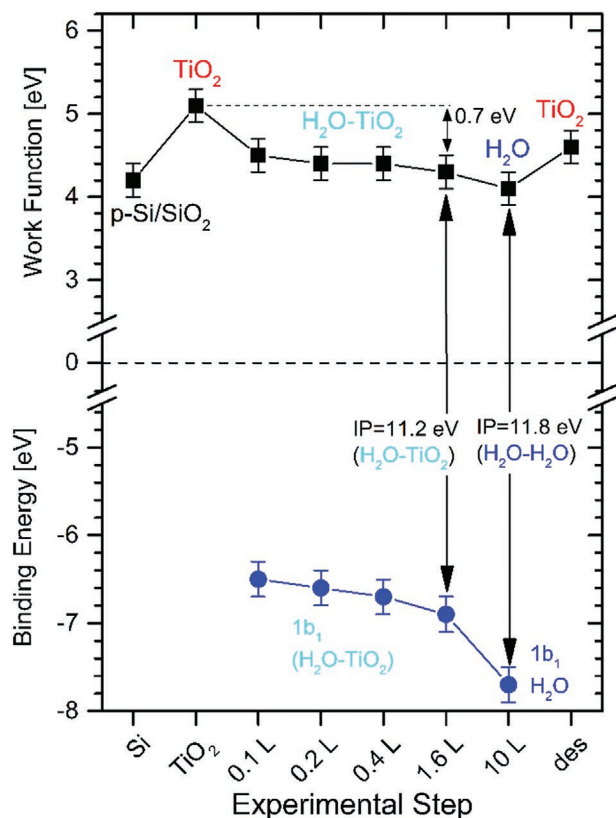

Figure 8. Evolution of the work function of the sample complemented by the ionization potentials IP of the $1b_1$-orbital of H_2O-TiO_2 and H_2O-H_2O molecular water species. In contrast to the usual convention, the binding energy scale is negative for a better visualization.

closely the observed binding energy shift of the surface water of 0.7 eV to lower binding energies in the O1s spectra and the UP valence band spectra compared to the bulk water. If the difference in work function is interpreted as surface dipole, this would hint at a surface water layer with oriented molecular dipoles, pointing away from the surface.

3. Conclusion

Cryo-photoelectron spectroscopy and electrochemical analysis techniques were used for the determination of the band structure of the p-Si/SiO_2/TiO_2/H_2O system. In summary, we studied the contact properties of the heterojunction formed by ALD-deposited TiO_2 on p-Si/SiO_2 and the interaction of the system with water. For p-Si a downward band bending of 0.3 eV was found at the interface. By combining the results of the water adsorption experiment, indicating the position of the valence band, and the Mott–Schottky analysis, which includes information about the position of the conduction band, a complete energy band diagram was constructed for the semiconductor/electrolyte interface. Furthermore, a direct correlation between the amount of surface hydroxide species, formed due to water dissociation, and Ti^{3+} defect state density is presented. Additionally, another surface water species can be identified besides the commonly found bulk molecular water.

4. Experimental Section

Atomic Layer Deposition of TiO_2: Thin films of amorphous TiO_2 were prepared on the native oxide of boron doped p-Si (100) samples (2.75 Ω cm, Silchem) by using a custom-built thermal ALD reactor. The substrates were cleaned 15 min with chloroform (≥99.9%, HPLC Plus, Sigma-Aldrich), 5 min with acetone, 5 min with ethanol and finally 5 min with Milli-Q water in an ultrasonic bath and dried in a nitrogen flow.[74] The silicon sample, which was used for the water adsorption experiment, was cleaned in a piranha bath instead using sulfuric acid (96%, VLSI Selectipur, BASF) and hydrogen peroxide (31%, VLSIn Selectipur, BASF) in a defined ratio ($H_2SO_4 : H_2O_2 = 3 : 1$) for 10 min, rinsed with Milli-Q water and dried in a nitrogen flow. After cleaning the silicon samples were loaded into the ALD reactor and stored under ultrahigh vacuum (UHV) conditions. The TiO_2 deposition was performed directly on the native oxide of the silicon. Titanium tetrachloride (99.995%, Sigma-Aldrich) and Milli-Q water were used as precursors for the ALD process. Both precursors were stored at room temperature and entered the reaction chamber alternating through pneumatic valves without using a carrier gas. The exposure times for titanium tetrachloride (first half-cycle) and water (second half-cycle) were 0.25 s and 0.3 s, respectively. During the process the pressure was monitored by a capacitive pressure gauge. The pumping unit for the ALD process consists of a backing pump and a LN2 cold trap. The deposition was carried out at a substrate temperature of 160 °C. To avoid condensing of the precursors, the $TiCl_4$ tube was heated at 30 °C and the H_2O tube and the reactor walls were maintained at 40 °C. High purity nitrogen (99.999%) was used as a purging gas with a flow rate of 20 sccm generating a nitrogen partial pressure of 0.5 torr during the process.

Interface Experiment: To study the contact properties between p-Si/SiO_2 and ALD-TiO_2, the thickness of the coating was increased stepwise. After deposition, the samples were transported within the integrated UHV system to the analysis chamber held at a base pressure of $5{\cdot}10^{-10}$ mbar, consisting of a XPS/UPS system (SPECS), equipped with a SPECS Phoibos 150 analyzer and a SPECS Focus 500 x-ray source using the monochromatized AlKα line at 1486.74 eV. The determination of the work function was performed with a bias-voltage of −3 V. The XPS measurements were recorded with the SpecsLab2 software. Each ALD deposition and the following XPS measurement were performed on boron doped silicon samples with the same specifications (dimension: 1 × 1 cm², orientation: (100), specific resistivity: 2.75 Ω cm). Besides the measurement of the pristine sample, five deposition steps were performed by applying 25, 50, 75, 100 and 300 cycles of ALD-TiO_2 on individual samples. The thicknesses of the grown TiO_2 films were determined by an imaging null ellipsometer (Accurion EP³ system). The ellipsometric measurements were performed with the program EP3View (Ver. 2.6). For the layer thickness modeling the program EP4Model (Ver. 1.2) was used.

Water Adsorption Experiment: Ultrapure water was filled into a Schlenk-type glass flask connected to a separated adsorption chamber with a base pressure of $1{\cdot}10^{-9}$ mbar. Freeze-pump cycling was used to purify the water. The dosage was controlled by a leak valve and the exposure time was varied stepwise to match the desired dosage from 0.1 L (Langmuir) to 10 L using uncorrected pressure readings. The sample was transferred on a LN-cooled manipulator from the adsorption chamber to the analysis chamber for consecutive cryo-photoelectron spectroscopy. The sample was not subject to light irradiation to avoid unwanted photocatalytic reactions during the experiment. For Cryo-UPS the HeI (21.2 eV) and HeII (40.8 eV) lines were employed. The p-Si/SiO_2 sample was deposited with 100 cycles of ALD-TiO_2, leading to a TiO_2 thickness of about 6 nm. The interface experiment started with the analysis of the pristine TiO_2 surface, followed by five deposition steps of frozen water leading to a nominal water dosage of 0.1 L, 0.2 L, 0.4 L, 1.6 L, and 10 L. At the end, the sample was slowly heated up to room temperature (RT) and measured again (desorption step).

Spectra Analysis: The Cryo-XP spectra were background subtracted using the Shirley method,[75] while for the Cryo-UP spectra a Tougaard

© 2021 The Authors. Advanced Materials Interfaces published by Wiley-VCH GmbH

Table 1. Full width at half-maximum (FWHM) and initial binding energies in eV for the $Ti2p_{3/2}$, O1s core level and UPS HeI components derived from Cryo-XPS and Cryo-UPS measurements.

Region	Component	FWHM [eV]	Binding Energy [eV]		
			Initial	Adsorption	Desorption
Ti2p	Ti^{4+}	1.0	458.9	458.8	459.2
	Ti^{3+}	1.0	457.4	457.3	457.7
O1s	TiO (O^{2-})	1.1	530.4	530.3	530.7
	SiO_2	1.1	532.0	531.9	532.3
	$Ti^{3+}(O_v)$-OH	1.1	–	532.6	532.6
	H_2O-TiO_2	1.1–1.5	–	533.2	–
	H_2O-H_2O	1.1–1.5	–	533.9	–
Si2p	$Si2p_{3/2}$	–	99.1	99.2	99.3
VB	VB_{max} (XPS)	–	3.2	3.1	3.4
	Ti^{3+}3d (HeI)	1.0	1.0	1.0	1.3

background was subtracted.[76] All Cryo-UP spectra were HeI- and HeII-satellite corrected, respectively. A sputtered Au foil served as reference sample in order to calibrate the spectrometer by making use of the Au $4f_{7/2}$ transition at 84.0 eV. The XPS core level peaks were fitted using a pseudo-Voigt function with a fixed ratio of 0.2 between the Lorentzian and Gaussian distributions. As a result, binding energy, line width, and intensity were obtained and compared on a qualitative basis. Beyond that, intensity changes within the same region (e.g., O1s) were treated on a quantitative basis since cross section and kinetic energy were unchanged. The full width at half-maximum (FWHM) and the initial binding energies for the deconvolution of the Ti2p and O1s core level are given in **Table 1**. The FWHM was calculated by peak fitting of the pristine spectrum. The larger values for the FWHM of the peaks related to H_2O are caused by the structurally less defined nature of these phases and the exact numerical values were optimized by the fitting routine. Additional information is provided in Section 2.3.

Mott–Schottky Analysis: For the Mott–Schottky analysis ITO coated glass (Alineason) was used as a substrate. First the substrates were cleaned with washing-up liquid to remove rough contaminations. After cleaning 10 min with acetone, 10 min with isopropanol and 10 min with Milli-Q water in an ultrasonic bath the samples were loaded into the ALD reactor and 300 cycles of TiO_2 were deposited with the same parameters described above, leading to a TiO_2 thickness of about 30 nm. To form an ohmic back contact the ITO was scratched and contacted with colloidal silver paste (Ted pella). The impedance of ALD-TiO_2 was measured in a Zahner PECC-2 cell with a Gamry potentiostat (Interface 1000) in a three-electrode setup with a silver/silver chloride (3 м NaCl) reference electrode and a platinum wire as a counter electrode at bias potentials ranging from 1.2 to 0 V versus RHE with an initial potential of 1.2 V versus RHE. Each 50 mV an electrochemical impedance spectrum was recorded with a frequency range of 100 000–0.1 Hz, an AC voltage of 10 mV (rms) and 25 points per decade. Before starting the impedance measurements, a pre-equilibration was performed at each potential for 10 min. As electrolyte solutions 0.1 м potassium hydroxide (Carl Roth) and 0.1 м sulfuric acid (Carl Roth) were used. The experiments were carried out in a dark box to avoid light disturbance. For data acquisition the Gamry framework program (Ver. 6.25) was used and the modeling was performed with the Gamry Echem Analyst software (Ver. 6.25).

Supporting Information

Supporting Information is available from the Wiley Online Library or from the author.

Acknowledgements

T.C. and M.F. contributed equally to this work. The manuscript was written through contributions of all authors. They all have given approval to the final version of the manuscript. Financial support through the DFG priority program SPP 1613 (JA 859/26-2) as well as by the project “fundamentals of electro-chemical phase boundaries at semiconductor/electrolyte interfaces” GEP-HE funded by the German Federal Ministry of Education and Research BMBF under contract 13XP5023A is gratefully acknowledged.

Open access funding enabled and organized by Projekt DEAL.

Conflict of Interest

The authors declare no conflict of interest.

Data Availability Statement

Research data are not shared.

Keywords

atomic layer deposition, energy band diagrams, photoelectron spectroscopy, water adsorption

Received: January 4, 2021
Revised: March 8, 2021
Published online: May 3, 2021

[1] T. Mayer, K. Schwanitz, B. Kaiser, A. Hajduk, M. V. Lebedev, W. Jaegermann, *J. Electron Spectrosc. Relat. Phenom.* **2017**, *221*, 116.
[2] W. Brown, W. Grannemann, *Solid-State Electron.* **1978**, *21*, 837.
[3] T. Fuyuki, H. Matsunami, *Jpn. J. Appl. Phys.* **1986**, *25*, 1288.
[4] L. Martinu, D. Poitras, *J. Vac. Sci. Technol., A* **2000**, *18*, 2619.
[5] X. Chen, S. S. Mao, *Chem. Rev.* **2007**, *107*, 2891.
[6] A. Fujishima, T. N. Rao, D. A. Tryk, *J. Photochem. Photobiol., C* **2000**, *1*, 1.
[7] B. J. Morgan, G. W. Watson, *J. Phys. Chem. C* **2010**, *114*, 2321.
[8] R. Liu, Z. Zheng, J. Spurgeon, X. Yang, *Energy Environ. Sci.* **2014**, *7*, 2504.
[9] T. Wang, Z. Luo, C. Li, J. Gong, *Chem. Soc. Rev.* **2014**, *43*, 7469.
[10] C. H. Heo, S.-B. Lee, J.-H. Boo, *Thin Solid Films* **2005**, *475*, 183.
[11] S. Vyas, R. Tiwary, K. Shubham, P. Chakrabarti, *Superlattices Microstruct.* **2015**, *80*, 215.
[12] M. Lottiaux, C. Boulesteix, G. Nihoul, F. Varnier, F. Flory, R. Galindo, E. Pelletier, *Thin Solid Films* **1989**, *170*, 107.
[13] K. S. Yeung, Y. W. Lam, *Thin Solid Films* **1983**, *109*, 169.
[14] L. M. Williams, D. W. Hess, *J. Vac. Sci. Technol., A* **1983**, *1*, 1810.
[15] R. L. Puurunen, *J. Appl. Phys.* **2005**, *97*, 121301.
[16] S. M. George, *Chem. Rev.* **2009**, *110*, 111.
[17] D. Bae, B. Seger, P. C. K. Vesborg, O. Hansen, I. Chorkendorff, *Chem. Soc. Rev.* **2017**, *46*, 1933.
[18] T. Cottre, K. Welter, E. Ronge, V. Smirnov, F. Finger, C. Jooss, B. Kaiser, W. Jaegermann, *Z. Phys. Chem.* **2020**, *234*, 1155.
[19] E. Ronge, T. Cottre, K. Welter, V. Smirnov, N. J. Ottinger, F. Finger, B. Kaiser, W. Jaegermann, C. Jooss, *Z. Phys. Chem.* **2019**, *234*, 1171.
[20] R. Wang, K. Hashimoto, A. Fujishima, M. Chikuni, E. Kojima, A. Kitamura, M. Shimohigoshi, T. Watanabe, *Adv. Mater.* **1998**, *10*, 135.
[21] T. L. Thompson, J. T. Yates, *Chem. Rev.* **2006**, *106*, 4428.

© 2021 The Authors. Advanced Materials Interfaces published by Wiley-VCH GmbH

21967350, 2021, 11, Downloaded from https://onlinelibrary.wiley.com/doi/10.1002/admi.202002257 by Technische Universitat Darmstadt, Wiley Online Library on [12/02/2024]. See the Terms and Conditions (https://onlinelibrary.wiley.com/terms-and-conditions) on Wiley Online Library for rules of use; OA articles are governed by the applicable Creative Commons License

[22] T. Wang, S. Liu, H. Li, C. Li, Z. Luo, J. Gong, *Ind. Eng. Chem. Res.* **2019**, *58*, 5510.
[23] T. Mayer, M. V. Lebedev, R. Hunger, W. Jaegermann, *J. Phys. Chem. B* **2006**, *110*, 2293.
[24] M. Fingerle, S. Tengeler, W. Calvet, T. Mayer, W. Jaegermann, *J. Electrochem. Soc.* **2018**, *165*, H3148.
[25] M. Fingerle, S. Tengeler, W. Calvet, W. Jaegermann, T. Mayer, *J. Electrochem. Soc.* **2020**, *167*, 136514.
[26] G. Ketteler, S. Yamamoto, H. Bluhm, K. Andersson, D. E. Starr, D. F. Ogletree, H. Ogasawara, A. Nilsson, M. Salmeron, *J. Phys. Chem. C* **2007**, *111*, 8278.
[27] R. L. Puurunen, *Chem. Vap. Deposition* **2003**, *9*, 327.
[28] A. G. Thomas, W. R. Flavell, A. K. Mallick, A. R. Kumarasinghe, D. Tsoutsou, N. Khan, C. Chatwin, S. Rayner, G. C. Smith, R. L. Stockbauer, S. Warren, T. K. Johal, S. Patel, D. Holland, A. Taleb, F. Wiame, *Phys. Rev. B* **2007**, *75*.
[29] J. Aarik, A. Aidla, T. Uustare, V. Sammelselg, *J. Cryst. Growth* **1995**, *148*, 268.
[30] J. Aarik, A. Aidla, H. Mändar, V. Sammelselg, *J. Cryst. Growth* **2000**, *220*, 531.
[31] J.-P. Niemelä, G. Marin, M. Karppinen, *Semicond. Sci. Technol.* **2017**, *32*, 093005.
[32] S. Haukka, E. L. Lakomaa, A. Root, *J. Phys. Chem.* **1993**, *97*, 5085.
[33] S. Haukka, E. L. Lakomaa, O. Jylha, J. Vilhunen, S. Hornytzkyj, *Langmuir* **1993**, *9*, 3497.
[34] U. Diebold, *Surf. Sci. Rep.* **2003**, *48*, 53.
[35] J. Klett, J. Ziegler, A. Radetinac, B. Kaiser, R. Schäfer, W. Jaegermann, F. Urbain, J.-P. Becker, V. Smirnov, F. Finger, *Phys. Chem. Chem. Phys.* **2016**, *18*, 10751.
[36] N. Kruse, S. Chenakin, *Appl. Catal., A* **2011**, *391*, 367.
[37] D. M. King, X. Du, A. S. Cavanagh, A. W. Weimer, *Nanotechnology* **2008**, *19*, 445401.
[38] I. A. Digdaya, L. Han, T. W. F. Buijs, M. Zeman, B. Dam, A. H. M. Smets, W. A. Smith, *Energy Environ. Sci.* **2015**, *8*, 1585.
[39] B. Enright, D. Fitzmaurice, *J. Phys. Chem.* **1996**, *100*, 1027.
[40] I. Iatsunskyi, M. Kempiński, G. Nowaczyk, M. Jancelewicz, M. Pavlenko, K. Załęski, S. Jurga, *Appl. Surf. Sci.* **2015**, *347*, 777.
[41] X. Chen, L. Liu, P. Y. Yu, S. S. Mao, *Science* **2011**, *331*, 746.
[42] D. Kuscer, J. Kovač, M. Kosec, R. Andriesen, *J. Eur. Ceram. Soc.* **2008**, *28*, 577.
[43] G. Wang, H. Wang, Y. Ling, Y. Tang, X. Yang, R. C. Fitzmorris, C. Wang, J. Z. Zhang, Y. Li, *Nano Lett.* **2011**, *11*, 3026.
[44] X. Liu, H. Xu, L. R. Grabstanowicz, S. Gao, Z. Lou, W. Wang, B. Huang, Y. Dai, T. Xu, *Catal. Today* **2014**, *225*, 80.
[45] T. K. Sham, M. S. Lazarus, *Chem. Phys. Lett.* **1979**, *68*, 426.
[46] T. Mayer, Dissertation Universität Berlin, **1993**.
[47] W. Göpel, J. A. Anderson, D. Frankel, M. Jaehnig, K. Phillips, J. A. Schäfer, G. Rocker, *Surf. Sci.* **1984**, *139*, 333.
[48] W. J. Lo, Y. W. Chung, G. A. Somorjai, *Surf. Sci.* **1978**, *71*, 199.
[49] C. A. Muryn, G. Tirvengadum, J. J. Crouch, D. R. Warburton, G. N. Raiker, G. Thornton, D. S. L. Law, *J. Phys.: Condens. Matter* **1989**, *1*, SB127.
[50] S. Eriksen, P. D. Naylor, R. G. Egdell, *Spectrochim. Acta Part A* **1987**, *43*, 1535.
[51] R. L. Kurtz, R. Stock-Bauer, T. E. Msdey, E. Román, J. De Segovia, *Surf. Sci.* **1989**, *218*, 178.
[52] P. B. Smith, S. L. Bernasek, *Surf. Sci.* **1987**, *188*, 241.
[53] F. J. Bustillo, E. Román, J. L. de Segovia, *Vacuum* **1989**, *39*, 659.
[54] V. E. Henrich, G. Dresselhaus, H. J. Zeiger, *Solid State Commun.* **1977**, *24*, 623.
[55] R. L. Kurtz, V. E. Henrich, *Phys. Rev. B* **1982**, *26*, 6682.
[56] C. A. Muryn, P. J. Hardman, J. J. Crouch, G. N. Raiker, G. Thornton, D. S. L. Law, *Surf. Sci.* **1991**, *251–252*, 747.
[57] J. M. Pan, B. L. Maschhoff, U. Diebold, T. E. Madey, *J. Vac. Sci. Technol., A* **1992**, *10*, 2470.
[58] M. B. Hugenschmidt, L. Gamble, C. T. Campbell, *Surf. Sci.* **1994**, *302*, 329.
[59] L.-Q. Wang, D. R. Baer, M. H. Engelhard, A. N. Shultz, *Surf. Sci.* **1995**, *344*, 237.
[60] M. A. Henderson, *Surf. Sci.* **1996**, *355*, 151.
[61] S. Wendt, P. T. Sprunger, E. Lira, G. K. H. Madsen, Z. Li, J. Ø. Hansen, J. Matthiesen, A. Blekinge-Rasmussen, E. Lægsgaard, B. Hammer, F. Besenbacher, *Science* **2008**, *320*, 1755.
[62] C. M. Yim, C. L. Pang, G. Thornton, *Phys. Rev. Lett.* **2010**, *104*, 036806.
[63] K. Schwanitz, U. Weiler, R. Hunger, T. Mayer, W. Jaegermann, *J. Phys. Chem. C* **2007**, *111*, 849.
[64] P. Reckers, M. Dimamay, J. Klett, S. Trost, K. Zilberberg, T. Riedl, B. A. Parkinson, J. Brötz, W. Jaegermann, T. Mayer, *J. Phys. Chem. C* **2015**, *119*, 9890.
[65] H. Li, Y. Guo, J. Robertson, *J. Phys. Chem. C* **2015**, *119*, 18160.
[66] S. Kashiwaya, T. Toupance, A. Klein, W. Jaegermann, *Adv. Energy Mater.* **2018**, *8*, 1802195.
[67] S. Hu, M. R. Shaner, J. A. Beardslee, M. Lichterman, B. S. Brunschwig, N. S. Lewis, *Science* **2014**, *344*, 1005.
[68] P. A. Thiel, T. E. Madey, *Surf. Sci. Rep.* **1987**, *7*, 211.
[69] K. S. Finnie, D. J. Cassidy, J. R. Bartlett, J. L. Woolfrey, *Langmuir* **2001**, *17*, 816.
[70] R. Sanjinés, H. Tang, H. Berger, F. Gozzo, G. Margaritondo, F. Lévy, *J. Appl. Phys.* **1994**, *75*, 2945.
[71] S. Hu, M. H. Richter, M. F. Lichterman, J. Beardslee, T. Mayer, B. S. Brunschwig, N. S. Lewis, *J. Phys. Chem. C* **2016**, *120*, 3117.
[72] S. Benkoula, O. Sublemontier, M. Patanen, C. Nicolas, F. Sirotti, A. Naitabdi, F. Gaie-Levrel, E. Antonsson, D. Aureau, F.-X. Ouf, S.-I. Wada, A. Etcheberry, K. Ueda, C. Miron, *Sci. Rep.* **2015**, *5*, 15088.
[73] H. Yang, E. Kim, S. H. Kim, M. S. Jeong, H. Shin, *Appl. Surf. Sci.* **2020**, *529*, 147020.
[74] C. Hess, R. Schlögl, *Nanostructured Catalysts: Selective Oxidations*, Royal Society of Chemistry, Cambridge **2011**.
[75] D. A. Shirley, *Phys. Rev. B* **1972**, *5*, 4709.
[76] S. Tougaard, *Surf. Interface Anal.* **1988**, *11*, 453.

© 2021 The Authors. Advanced Materials Interfaces published by Wiley-VCH GmbH

21967350, 2021, 11, Downloaded from https://onlinelibrary.wiley.com/doi/10.1002/admi.202002257 by Technische Universitat Darmstadt, Wiley Online Library on [12/02/2024]. See the Terms and Conditions (https://onlinelibrary.wiley.com/terms-and-conditions) on Wiley Online Library for rules of use; OA articles are governed by the applicable Creative Commons License